AD_____

Award Number: DAMD17-01-1-0326

TITLE: Automated Method for Analysis of Mammographic Breast Density - A Technique for Breast Cancer Risk Estimation

PRINCIPAL INVESTIGATOR: Heang-Ping Chan, Ph.D.

CONTRACTING ORGANIZATION: University of Michigan
Ann Arbor, Michigan 48109-1274

REPORT DATE: July 2004

TYPE OF REPORT: Annual

PREPARED FOR: U.S. Army Medical Research and Materiel Command
Fort Detrick, Maryland 21702-5012

DISTRIBUTION STATEMENT: Approved for Public Release;
Distribution Unlimited

The views, opinions and/or findings contained in this report are those of the author(s) and should not be construed as an official Department of the Army position, policy or decision unless so designated by other documentation.

20050105 027

REPORT DOCUMENTATION PAGE

Form Approved
OMB No. 074-0188

Public reporting burden for this collection of information is estimated to average 1 hour per response, including the time for reviewing instructions, searching existing data sources, gathering and maintaining the data needed, and completing and reviewing this collection of information. Send comments regarding this burden estimate or any other aspect of this collection of information, including suggestions for reducing this burden to Washington Headquarters Services, Directorate for Information Operations and Reports, 1215 Jefferson Davis Highway, Suite 1204, Arlington, VA 22202-4302, and to the Office of Management and Budget, Paperwork Reduction Project (0704-0188), Washington, DC 20503

1. AGENCY USE ONLY (Leave blank)	2. REPORT DATE July 2004	3. REPORT TYPE AND DATES COVERED Annual (1 July 2003 – 30 June 2004)

4. TITLE AND SUBTITLE
Automated Method for Analysis of Mammographic Breast Density – A Technique for Breast Cancer Risk Estimation

5. FUNDING NUMBERS
DAMD17-01-1-0326

6. AUTHOR(S)
Heang-Ping Chan, Ph.D.

7. PERFORMING ORGANIZATION NAME(S) AND ADDRESS(ES)
University of Michigan
Ann Arbor, Michigan 48109-1274

E-Mail: chanhp@umich.edu

8. PERFORMING ORGANIZATION REPORT NUMBER

9. SPONSORING / MONITORING AGENCY NAME(S) AND ADDRESS(ES)
U.S. Army Medical Research and Materiel Command
Fort Detrick, Maryland 21702-5012

10. SPONSORING / MONITORING AGENCY REPORT NUMBER

11. SUPPLEMENTARY NOTES

12a. DISTRIBUTION / AVAILABILITY STATEMENT
Approved for Public Release; Distribution Unlimited

12b. DISTRIBUTION CODE

13. ABSTRACT (Maximum 200 Words)

The goal of this proposed project is to develop an automated technique to assist radiologists in estimating mammographic breast density. The computerized image analysis tool can provide a consistent and reproducible estimation of percent dense area on routine clinical mammograms, thereby contributing to the understanding of the relationship of mammographic density to breast cancer risk, detection, and prognosis, and the prevention and treatment of breast cancer.

During this project year, we completed the observer performance study that compared the mammographic density on digital mammograms (DMs) and digitized film mammograms (DFMs) manually segmented by experienced radiologists. The average mammographic density on digital mammograms was found to be significantly lower than that on digitized mammograms as perceived by radiologists. The lower density on DMs may improve the mammographic sensitivity for lesion detection on dense breasts. However, for patients with DFMs and DMs taken over time, comparison of serial mammograms for breast density changes will be problematic.

We also performed a study to compare mammographic density segmented from DMs by our automated density segmentation program, referred to as Mammographic Density ESTimator (MDEST), with the average mammographic density manually segmented by four experienced radiologists. The mammographic density from DMs obtained by our automated MDEST program is highly correlated with the average mammographic density manually segmented by radiologists. The study therefore indicates the feasibility of using our MDEST program for estimation of mammographic density, although improvement is needed to further increase the segmentation accuracy. We will continue to improve the image analysis methods in the coming year.

14. SUBJECT TERMS
breast cancer, mammography, breast density, computer-assisted analysis, automated segmentation, risk monitoring

15. NUMBER OF PAGES
30

16. PRICE CODE

17. SECURITY CLASSIFICATION OF REPORT Unclassified	18. SECURITY CLASSIFICATION OF THIS PAGE Unclassified	19. SECURITY CLASSIFICATION OF ABSTRACT Unclassified	20. LIMITATION OF ABSTRACT Unlimited

NSN 7540-01-280-5500

Standard Form 298 (Rev. 2-89)
Prescribed by ANSI Std. Z39-18
298-102

(3)   Table of Contents

     (A)   Collection of a Database of Full Field Digital Mammograms (DMs) and Digitized Mammograms (DFM)

     (B)   Comparison of Percent Mammographic Density Estimated on Full Field Digital Mammograms and Digitized Screen-Film Mammograms

     (C)   Automated Segmentation of Dense areas on Digital Mammograms

(4)   Introduction

Previous studies have found that there is a strong correlation between mammographic breast density and the risk of breast cancer. Mammographic breast density has been used by researchers in many studies to estimate breast cancer risk of epidemiological factors, monitor the effects of preventive treatments such as tamoxifen or dietary interventions, monitor the breast cancer risk of hormone replacement therapy, and investigate factors affecting mammographic sensitivity and cancer prognosis. However, most studies used Breast Imaging Reporting and Data System (BI-RADS) density rating as a measure of mammographic breast density, which contributes large inter- and intraobserver variations and may reduce the sensitivity of the analysis.

The goal of this proposed project is to develop a fully automated technique to assist radiologists in estimating mammographic breast density. We hypothesize that the computerized technique can accurately and efficiently segment the dense area on digitized or digital mammograms, thereby eliminating inter- and intra-observer variations. The dense area as a percentage of total breast area thus estimated will be more consistent and reproducible than radiologists' subjective BI-RADS rating. To accomplish this goal, we will (1) collect a large database of mammograms, including digitized film mammograms and digital mammograms, for training and testing the dense area segmentation program; (2) evaluate the correlation between the radiologists' breast density classification based on BI-RADS lexicon and the percent breast dense area; and (3) study the correlation of percent breast dense area between different views of the same breast and between the same view of the two breasts; and (4) investigate the correlation between the percent breast dense area estimated from mammograms and the volumetric dense breast tissue estimated from a data set of magnetic resonance (MR) breast images. These comparisons will provide important information regarding the consistency of the BI-RADS rating with the measured percent breast dense area, the appropriate measure of % dense area from different mammographic views, and the usefulness of using the percent breast dense area on mammograms as an indicator of volumetric breast tissue density.

It is expected that this project will produce a fully automated and effective tool for analysis of mammographic breast density, which can be applied to routinely acquired mammograms without special calibrations. This will facilitate studies of various factors associated with breast cancer risk and mammographic sensitivity, and monitoring the effects of interventional or preventive strategies. The image analysis tool will therefore contribute to the understanding of the relationship of density to breast cancer risk, detection, prognosis, and to the prevention and treatment of breast cancer.

(5) Body

The current year (7/1/03-6/30/04) is the third year of the project. We requested and obtained approval for a one-year no-cost time extension. Therefore, this is an annual progress report instead of the final report. We will describe in the following details of the studies that we performed this year.

(A) Collection of a Database of Full Field Digital Mammograms (DMs) and Digitized Mammograms (DFM)

In this project year, we continued to enlarge the data set of full field direct digital mammograms acquired from a GE Senographe 2000D system. A data set of 99 patients with 101 pairs of digital mammogram (DM) and digitized screen-film mammogram (DFM) obtained from the same patients have been collected to date. This data set was used in two studies for development of a breast density analysis tool for digital mammograms. In the first study, radiologists segmented the mammographic density on the DMs and the DFMs using interactive thresholding. The mammographic density perceived by radiologists on the two types of mammograms of the same patient was compared. In the second study, a computerized breast density segmentation program developed for the DFMs was directly applied to DMs and the computer's density segmentation was compared with that by radiologists. This study was designed to evaluate the segmentation performance and obtain information how to adapt the mammographic density segmentation program to DMs.

(A) Comparison of Percent Mammographic Density Estimated on Full Field Digital Mammograms and Digitized Screen-Film Mammograms

We are comparing image information on DMs and DFMs for radiologist's interpretation and computerized image analysis. In last year's report, we discussed a preliminary study for the comparison of mammographic density estimated on DMs and DFMs. In this year, we completed the study and presented the results at the 89th Scientific Assembly and Annual Meeting of the Radiological Society of North America held in December of 2003 in Chicago. The study is summarized in the following.

(a) Data Set

Two hundred and two pairs of DM and DFM were collected with IRB approval from 99 patients. Each case contains the craniocaudal (CC) view and the mediolateral oblique (MLO) view. The time interval between the DM and DFM ranged from 0 to 118 days (mean=26.3 days). The DFMs were acquired with GE DMR systems and the DMs were acquired with the GE Senographe 2000D system. Both the DMs and the DFMs were acquired with automated exposure techniques that selected the appropriate target, filter, and kVp. The DFMs were digitized with a laser film scanner.

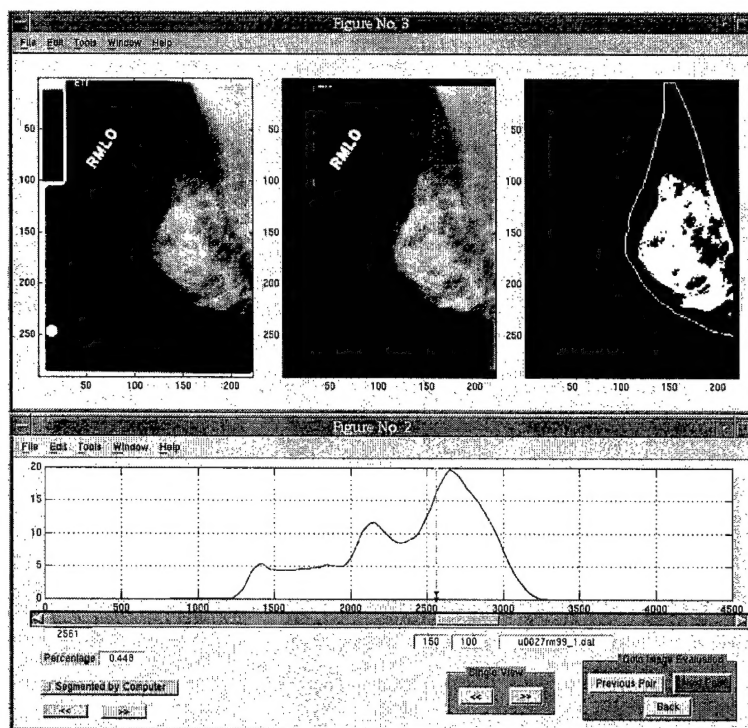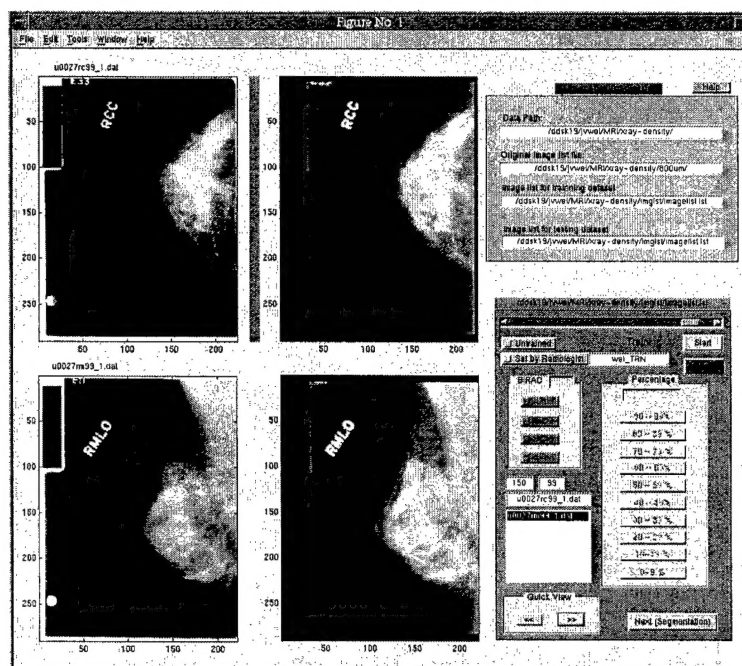### (b) Graphical User Interface for Segmentation of Breast Density on Digital Mammograms

Fig. 1. Graphical user interface for segmentation of breast density on digital or digitized mammograms. Upper: First screen that shows the two-view mammograms together. Lower: the second screen that shows one view at a time, and the histogram and thresholded image for user reference during interactive thresholding.

We have previously developed a graphical user interface (GUI) for interactive thresholding of dense tissue regions on DFMs. The GUI is used in observer experiments so that radiologists can segment the mammograms manually and provide a gold standard for developing automated computerized segmentation methods. We have modified the GUI for DFMs to be used with DMs. In this study, we used the new GUI for DMs to manually segment a data set of DMs. The results are compared with manual segmentation of DFMs of the same patients in our data set described above, using the previously developed GUI.

(b) Methods

The breast boundaries on the DMs and DFMs were detected automatically by the computer. The mammograms were displayed on a workstation with the GUI as shown in Fig. 1 The DFMs are processed with a dynamic range compression technique to reduce the gray level range of the image. For the DMs, we used the processed GE DM image as input. The gray level histogram of the breast region is displayed and the observer can adjust the gray level threshold interactively to segment the dense region from the fatty region. The segmented image (binary image with dense region in white and fatty region in black) is shown on the display virtually in real time while the threshold is being adjusted. The observer can then change the threshold until he/she is satisfied that the segmented region is similar to the dense region seen on the gray level mammogram by subjective judgment. The DMs and DFMs were mixed but the DM and the DFM from the same patient were separated by at least 10 other mammogram pairs. In this way, the observer would not be able to compare the density of the corresponding DM and DFM. The mammographic density was estimated as the percent dense area relative to the breast area, excluding the pectoral muscle in the MLO views. Five Mammography Quality Standards Act (MQSA) qualified radiologists participated as observers in the experiment.

(c) Results

Fig. 2 shows the comparison of the percent breast density on the data set of 99 pairs of digitized DFMs and DMs for CC and MLO views segmented by an experienced radiologist. The slope of the linear regression line to the scatter plot is greater than 1 for both views.

Fig. 3 shows the difference in the percent breast density between the DFM and the DM from the same breast and the same view. Most of the differences are greater than 0. Fig. 4 shows the ratio of the percent breast density on DFM to that on the corresponding DM. Most of the ratios are greater than 1. These results indicate that the mammographic density estimated from DFMs are on average lower than that from DFMs, Table 1 summarized the results for the 5 radiologists. Four of the five radiologists found that the mammographic density on the DFM is higher than that on the corresponding DMs. The mean difference in the segmented density was about 3.5% and the mean ratio was about 1.30, indicating that the mammographic density appears to be 30% higher, on average, on the DFMs. The difference in the estimated mammographic density was found to be statistically significant ($p<0.05$) by a paired t-test.

Since the DFM and the corresponding DM were taken within a relatively short period of time. The breast tissue density should not change very much on average. The difference in the mammographic density may be attributed to the harder beam quality used and the digital image processing applied to the DMs. The lower density may improve the mammographic sensitivity

for lesion detection on dense breasts. However, for patients with DFMs and DMs taken over time, comparison of serial mammograms for breast density changes will be problematic.
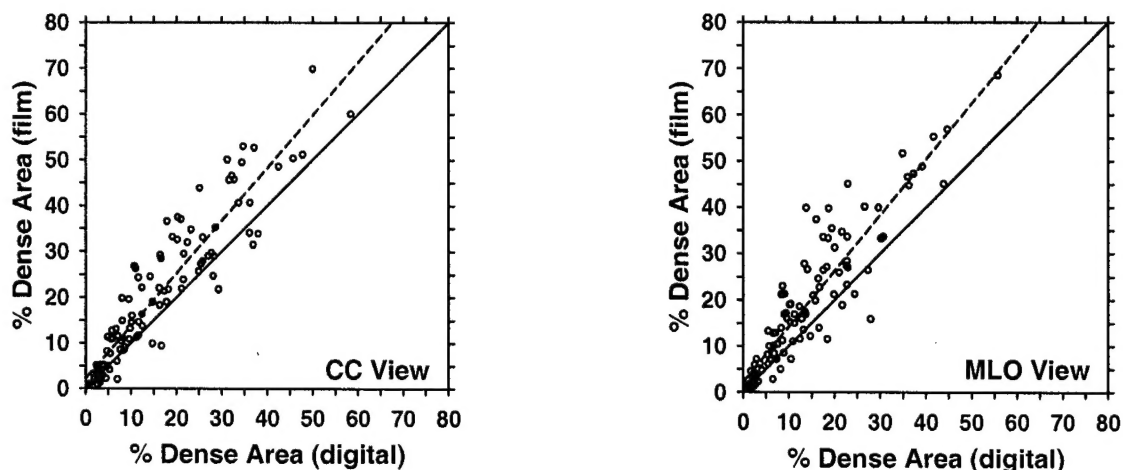

Fig. 2. Comparison of the percent mammographic density from the digital and digitized mammograms segmented by an experienced radiologist. The dashed line is the linear regression curveThe percent density from digitized mammograms are generally higher than those from digital mammograms.
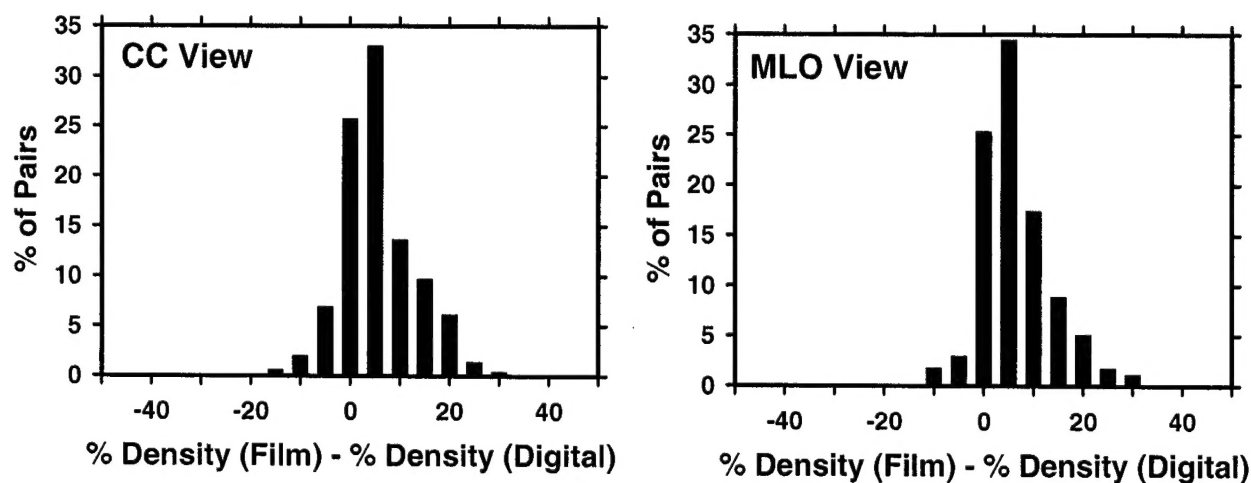

Fig. 3. Difference in percent mammographic density between the digitized and the digital mammogram of the same breast and the same view segmented by 5 radiologists. The percent density from digitized mammogram is on average higher than that from the digital mammogram.
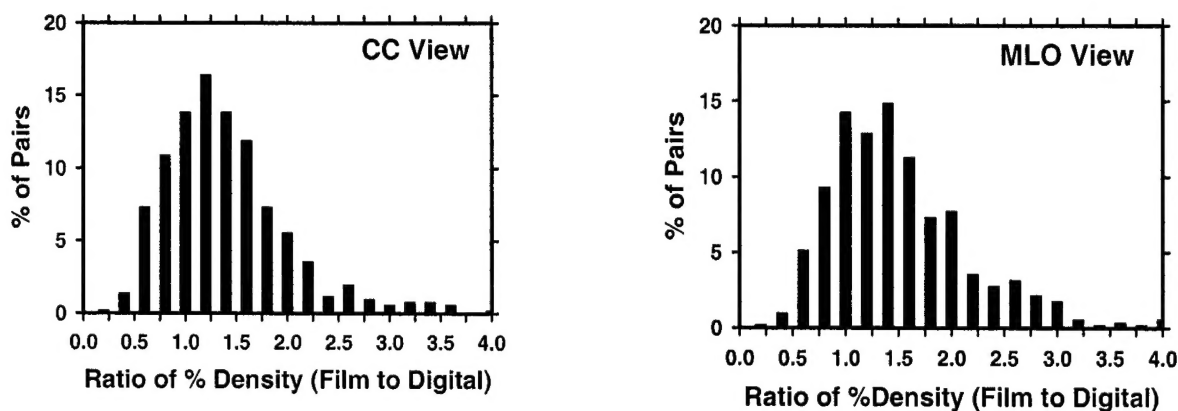
Fig. 4.   Ratio of percent mammographic density from the digitized mammogram to that from the corresponding digital mammogram segmented by 5 radiologists. Most of the ratios are greater than 1, indicating that the percent density from digitized mammogram is on average higher than that from the digital mammogram.

Table 1.   The mean difference and mean ratio of percent mammographic density estimated on DFMs and DMs by 5 experienced radiologists. The results indicated that four of the five radiologists perceived a higher density on DFMs than that on DMs. The average results are found to be statistically significant (p<0.05) by paired t-test over the group of radiologists.

Radiologist	Mean Difference in % Density (Film – Digital)	Mean Ratio of % Density (Film / Digital)
Rad 1	4.92	1.35
Rad 2	5.50	1.53
Rad 3	4.63	1.39
Rad 4	4.66	1.35
Rad 5	-2.01	0.88
Average (all)	3.54	1.30
Average (#1 - #4)	4.93	1.40

(B)   Automated Segmentation of Dense areas on Digital Mammograms

In the previous project years, we developed a computerized system, mammographic density estimator (MDEST) (Zhou et al. 2001), to estimate breast density automatically on digitized film mammograms (DFM). The MDEST system performs dynamic range compression, breast boundary tracking, pectoral muscle trimming for MLO view, gray level thresholding based on histogram analysis, and calculation of the percent dense area on the mammogram. In the previous study, 260 digitized 4-view mammograms of 65 patients were used. The gold standard of percent dense area of the breast region for each mammogram was obtained by averaging five

Page 9

radiologists' manually segmented percent dense area. We found that the correlation between the computer-estimated percent dense area and radiologists' manual segmentation was 0.94 and 0.91, with root-mean-square (RMS) errors at 6.1% and 7.2%, respectively, for CC and MLO views.

In this study, we investigate the feasibility of computerized mammogramic density estimation on DMs and DFMs using the same image segmentation system. The MDEST system was directly applied to the DM and the corresponding DFM without any re-training except that the preprocessing filter was modified for DMs. The performance was evaluated by analyzing the correlation between the computer-estimated mammographic density and the gold standard obtained by radiologists' interactive thresholding.

(a) Data Set

The data set described in Section (A) above was used in this study. The preprocessed image was downsized to a pixel size of 800 µm x 800 µm image and 4096 gray levels. was digitized with a LUMISYS 85 laser film scanner with a pixel size of 50 µm x 50 µm and 4096 gray levels. The digitized mammogram was also downsized to a 800 µm x 800 µm image using a 16x16 box filter.

(b) Methods

Our previously developed computerized system MDEST was applied to the DMs and DFMs to estimate the mammographic density without any re-training. The density estimation was performed in three stages: breast region segmentation, image enhancement, and gray level thresholding based on histogram analysis . First, the breast region was segmented from the surrounding background by an automated breast boundary tracking algorithm for DFM. For DM, thresholding was used to separate the breast region from the background. Since our current pectoral muscle trimming program is not 100% accurate, the pectoral muscle was manually trimmed on the MLO view images for both DFM and DM in this study in order to separate the errors due to breast density segmentation from those due to pectoral muscle trimming. Second, an adaptive dynamic range compression technique was applied to enhance the DFM image. For DM image, a Laplacian pyramid multi-resolution preprocessing method (Wei et al. 2004) was used for image enhancement. At the third stage, for both DM and DFM, rule-based classification was used to classify the breast image into one of four classes according to the characteristic features of its gray level histogram (Zhou et al. 2001). For each image in the classified classes, a gray level threshold was determined adaptively to segment the dense area from the breast region. The breast density was estimated as the percentage of the segmented dense area relative to the breast area. To evaluate the performance of MDEST, the computer segmentation results were compared to those by manual segmentation with interactive thresholding by MQSA radiologists. The "gold standard" of percent dense area for each mammogram was obtained by averaging the manually segmented percent dense areas of four of the radiologists. The results of one of the radiologists who perceived the DMs as more dense than the DFMs was not included because that appeared to be an outlier.

(c) Results

Fig. 5(a)-(d) show the comparison of the percent dense area between the estimation by the MDEST system and the gold standard on DM and DFM for CC- and MLO-view mammograms, respectively. Table 2 summarizes the comparison between the MDEST performance and the gold standard for DM and DFM, respectively. The correlation between the computer-estimated percent dense area and the gold standard is 0.850 and 0.873 on DM, and 0.885 and 0.824 on DFM, for CC and MLO views, respectively. For all of the images combining CC- and MLO-views, the correlation is 0.859 and 0.855 on DM and DFM, respectively. The RMS difference in the percent dense area between the MDEST estimation and the gold standard is 7.26%, 5.70% and 6.52% on DM, and 6.87%, 8.16% and 7.54% on DFM for CC-view alone, MLO-view alone, and combined CC and MLO-views, respectively.
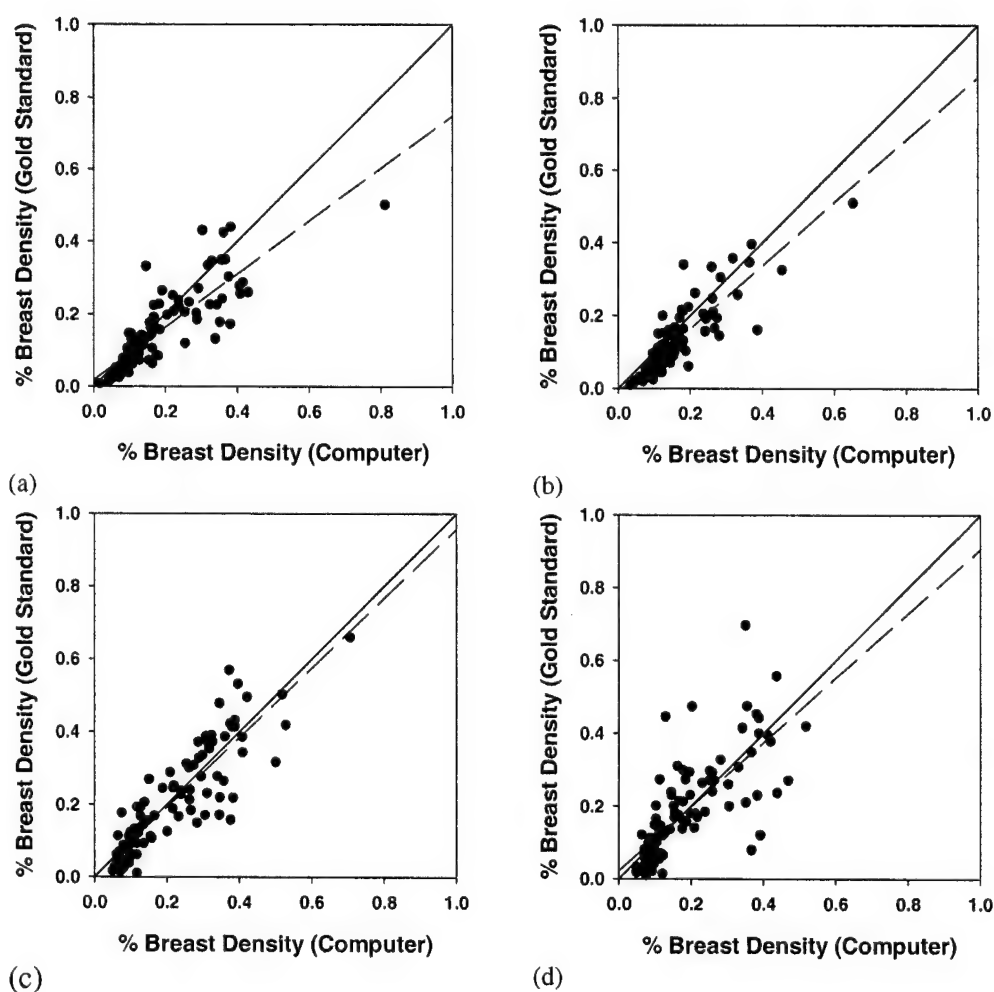

(a) (b) (c) (d)

Figure 5. Comparison of the percent dense area between the estimation by the MDEST system and the gold standard. The dashed line represents the linear regression of the data on the plot. (a) DM CC view, (b) DM MLO view, (c) DFM CC view, (d) DFM MLO view.

Table 2. The correlation and RMS difference between the estimated percent dense area by the MDEST system and the gold standard (average of four MQSA radiologists).

Image subsets	DM		DFM	
	Correlation	RMS Error	Correlation	RMS Error
CC view	0.850	7.26%	0.885	6.87%
MLO view	0.873	5.70%	0.824	8.16%
All images	0.859	6.52%	0.855	7.54%

(d)   Discussion

This preliminary study demonstrated that the estimation of mammographic density could be performed efficiently by our automated image analysis tool. The computer-estimated percent dense area had a high correlation with the gold standard obtained from averaging four MQSA radiologists' manual segmentation. The results also demonstrated the feasibility of estimating breast density automatically on DM and DFM using the same MDEST system. However, it can also be observed that some mammograms were not segmented accurately and the percent density deviated relatively far from the diagonals. Improvement in the MDEST method will be needed to increase the breast density segmentation accuracy. We will continue to investigate methods to improve the segmentation in the coming project year.

(6)   Key Research Accomplishments

- Continue to collect the data sets of digitized film mammograms and digital mammograms for development of the automated density segmentation program (Task 1).

- Complete an observer performance study with five MQSA radiologists in manual segmentation of the digitized film mammograms and digital mammograms (Task 2 and Task 4).

- Compare the mammographic density segmented from DFMs and DMs to evaluate the similarity or differences of the properties between DFMs and DMs (Task 2 and Task 4).

- Develop a Graphical User Interface (GUI) for interactive segmentation of full field direct digital mammograms (Task 4)

- Compare automated density segmentation results on DMs with MQSA radiologists' manual segmentation and evaluate the performance of the automated program (Task 2 and Task 4).

(7)   Reportable Outcomes

As a result of the support by the USAMRMC BCRP grant, we have conducted studies to investigate the correlation between the mammographic density on digital mammograms and digitized film mammograms, and evaluate the performance of the automated mammographic density segmentation program for digital mammograms. We have presented the results of these investigations in this project year. The journal article that we submitted last year was also published.

Journal Articles:

Wei J, Chan HP, Helvie MA, Roubidoux MA, Sahiner B, Hadjiiski L, Zhou C, Paquerault S, Chenevert T, Goodsitt MM. Correlation between Mammographic Density and Volumetric Fibroglandular Tissue Estimated on Breast MR Images. Medical Physics 2004; 31: 933-942.

Conference Proceeding:

Zhou C, Chan HP, Wei J, Helvie MA, Roubidoux MA, Paramagul C, Nees A, Hadjiiski LM, Sahiner B. Performance evaluation of an automated breast density estimation system for digital mammograms and digitized film mammograms. In: Digital Mammography IWDM 2004: 7th International Workshop on Digital Mammography. Ed. Pisano E. (in press).

Conference Presentation:

Zhou C, Hadjiiski LM, Sahiner B, Chan HP, Helvie MA, Wei, J. Computerized mammographic breast density estimation: Expectation-Maximization estimation and neural network classification of breast density. Presented at the 89th Scientific Assembly and Annual Meeting of the Radiological Society of North America, Chicago, IL, November 30-December 5, 2003. RSNA Program 2003; 389.

Zhou C, Chan HP, Wei J, Helvie MA, Roubidoux MA, Paramagul C, Nees A, Hadjiiski LM, Sahiner B. Performance evaluation of an automated breast density estimation system for digital mammograms and digitized film mammograms. Presented at the 7th International Workshop on Digital Mammography. IWDM-2004. Durham, North Carolina. June 18-21, 2004.

(8)   Conclusions

During this project year, we completed the observer study that compared the mammographic density manually segmented by 5 experienced radiologists from DFMs and DMs. We found that, on average, the mammographic density estimated from DMs is significantly lower than that estimated from DFMs. The differences in the mammographic density between the two modalities may be attributed to the harder beam quality used and image processing applied to the DMs. The lower density on DMs may improve the mammographic sensitivity for lesion detection on dense breasts. However, for patients with DFMs and DMs taken over time, comparison of serial mammograms for breast density changes will be problematic.

We also performed a study to compare mammographic density segmented from DMs by our automated density segmentation program, referred to as Mammographic Density ESTimator (MDEST), with the average mammographic density manually segmented by four experienced radiologists. The mammographic density from DMs obtained by our automated MDEST program is highly correlated with the average mammographic density manually segmented by radiologists. The results indicate the feasibility of using our automated MDEST for estimation of mammographic density, although further investigations are still needed to improve the accuracy of the segmentation program.

If successfully developed, the computerized image analysis tool can provide a consistent and reproducible estimation of percent dense area on routine clinical mammograms. The automated image analysis tool may improve the sensitivity of quantifying mammographic density changes, thereby contributing to the understanding of the relationship of mammographic density to breast cancer risk, detection, and prognosis, and the prevention and treatment of breast cancer.

(9)   References

1. Zhou C, Chan HP, Petrick N, Helvie MA, Goodsitt MM, Sahiner B, Hadjiiski LM. Computerized image analysis: Estimation of breast density on mammograms. Medical Physics 2001; 28: 1056-1069.

(10)   Appendix

Copies of the following publications are enclosed with this report:

Journal Articles:

Wei J, Chan HP, Helvie MA, Roubidoux MA, Sahiner B, Hadjiiski L, Zhou C, Paquerault S, Chenevert T, Goodsitt MM. Correlation between Mammographic Density and Volumetric Fibroglandular Tissue Estimated on Breast MR Images. Medical Physics 2004; 31: 933-942.

Conference Proceeding:

Zhou C, Chan HP, Wei J, Helvie MA, Roubidoux MA, Paramagul C, Nees A, Hadjiiski LM, Sahiner B. Performance evaluation of an automated breast density estimation system for digital mammograms and digitized film mammograms. In: Digital Mammography IWDM 2004: 7th International Workshop on Digital Mammography. Ed. Pisano E. (in press).

Correlation between mammographic density and volumetric fibroglandular tissue estimated on breast MR images

Jun Wei,[a)] Heang-Ping Chan, Mark A. Helvie, Marilyn A. Roubidoux, Berkman Sahiner, Lubomir M. Hadjiiski, Chuan Zhou, Sophie Paquerault, Thomas Chenevert, and Mitchell M. Goodsitt
Department of Radiology, University of Michigan, Ann Arbor, Ann Arbor, Michigan 49109

Previous studies have found that mammographic breast density is highly correlated with breast cancer risk. Therefore, mammographic breast density may be considered as an important risk factor in studies of breast cancer treatments. In this paper, we evaluated the accuracy of using mammograms for estimating breast density by analyzing the correlation between the percent mammographic dense area and the percent glandular tissue volume as estimated from MR images. A dataset of 67 cases having MR images (coronal 3-D SPGR T1-weighted pre-contrast) and corresponding 4-view mammograms was used in this study. Mammographic breast density was estimated by an experienced radiologist and an automated image analysis tool, Mammography Density ESTimator (MDEST) developed previously in our laboratory. For the estimation of the percent volume of fibroglandular tissue in breast MR images, a semiautomatic method was developed to segment the fibroglandular tissue from each slice. The tissue volume was calculated by integration over all slices containing the breast. Interobserver variation was measured for 3 different readers. It was found that the correlation between every two of the three readers for segmentation of MR volumetric fibroglandular tissue was 0.99. The correlations between the percent volumetric fibroglandular tissue on MR images and the percent dense area of the CC and MLO views segmented by an experienced radiologist were both 0.91. The correlation between the percent volumetric fibroglandular tissue on MR images and the percent dense area of the CC and MLO views segmented by MDEST was 0.91 and 0.89, respectively. The root-mean-square (rms) residual ranged from 5.4% to 6.3%. The mean bias ranged from 3% to 6%. The high correlation indicates that changes in mammographic density may be a useful indicator of changes in fibroglandular tissue volume in the breast. © *2004 American Association of Physicists in Medicine.* [DOI: 10.1118/1.1668512]

Key words: mammography, breast density, MR images, correlation

I. INTRODUCTION

Studies have shown that there is a strong positive correlation between breast parenchymal density imaged on mammograms and breast cancer risk.[1–3] The relative risk is estimated to be about 4 to 6 for women whose mammograms have parenchymal densities over 60% of the breast area, as compared to women with less than 5% densities. Other cohort studies[4–13] also found that breast cancer risk in the category with the most extensive dense tissue was 1.8 to 6 times as high as that in the category with the least extensive dense tissue. Mammographic density as the risk indicator is greater than almost all other risk factors of breast cancer.[2,14] Although there is no direct evidence that changes in mammographic breast densities will result in changes in breast cancer risk, the strong correlation between breast density and breast cancer risk has prompted researchers to use mammographic density for monitoring the effects of intervention as well as for studying breast cancer etiology.[14–17]

A number of researchers have investigated image analysis techniques to estimate breast density.[15,18–28] The common approaches are to analyze the textural pattern or the percentage of mammographic densities relative to the breast area. It has been found that the texture measures were correlated with parenchymal density patterns but they appeared to be less sensitive measures of relative risk than the percent dense area.[1,25,29] In current practice, breast density is estimated mainly by radiologists' visual judgment of the fibroglandular tissue imaged on mammograms following the Breast Imaging—Reporting and Data System (BI-RADS) lexicon.[30,31] Because of the qualitative and subjective nature of visual judgment, there are large intraobserver and interobserver variations in the estimated breast density. The large variability may reduce the observed correlation between breast cancer risk and breast density. It may also reduce the sensitivity of studies using mammographic density for monitoring the effect of risk modifying treatments. We have developed an automated image analysis system, Mammographic Density ESTimator (MDEST), to assist radiologists in estimating breast density on mammograms. A computerized analysis is expected to increase the reproducibility and consistency in the estimation of mammographic density, thereby improving the accuracy of the related studies. In our previous study, we have found that the percent mammographic density segmented by MDEST agreed closely with that estimated by radiologists' interactive thresholding.[32]

The high correlation between breast cancer risk and breast

density indicates that breast cancer risk may be closely related to the volume of glandular tissue in the breast. Among the modalities available for breast imaging at present, magnetic resonance (MR) imaging is likely to be the most accurate method for volumetric dense tissue estimation because fibroglandular tissue and adipose tissue can be well distinguished in MR images when a proper image acquisition technique is used.[33] However, MR imaging is expensive, making it difficult to use MR imaging as a routine monitoring tool.[33,34] On the other hand, a mammogram is a two-dimensional (2-D) projection image of a three-dimensional (3-D) object. The area of dense tissue measured on a mammogram is not an accurate measure of the volume of fibroglandular tissue in the breast because no thickness information is used. However, mammography is a widely available low cost procedure that may be used for monitoring breast density change during preventive and interventional treatment or other studies. Women who participate in screening will also have mammograms readily available for retrospective review. Therefore, mammography will most likely be the method of choice for breast density estimation.

In this study, we investigated the correlation between the volumetric fibroglandular tissue in the breast and the projected breast dense area on mammograms by analyzing the percent volumetric fibroglandular tissue in MR breast images and the percent dense area in corresponding mammograms. Our purpose in this study is not to evaluate the usefulness of either MR fibroglandular tissue volume or mammographic density as an indicator for breast cancer risk, which have been studied by other investigators. Rather, we used the MR breast images to estimate the volumetric fibroglandular tissue in the breast and explored the reason that a change in mammographic density (2-D) can be used as an indicator of breast density change (3-D). These comparisons will provide a better understanding of their relationship, and may lead to improved methods for utilizing mammographic density as a surrogate marker for breast cancer risk.

II. MATERIALS AND METHOD

A. Dataset

In a previous study, gadolinium contrast enhanced MR dynamic imaging was employed to characterize malignant and benign breast lesions. A dataset was collected with IRB approval which included MR images and corresponding mammograms acquired between detection and before biopsy for a given patient. In the MR study, several series of images were acquired for each patient. Patients were scanned prone using a commercial dual phased-array breast coil. The imaging protocol included a series was the coronal 3-D T1-weighted pre-contrast series (coronal sections 2–5 mm thick, 32 slices; 3-D Spoiled Gradient-Recalled Echo (SPGR); TE = 3.3 ms; TR = 10 ms, Flip = 40°, matrix = 256×128, FOV = 28–32 cm right/left, 14–16 cm superior/inferior, scan time = 2 min 38 sec). This 3-D SPGR sequence produces full volume coverage of both breasts with contiguous image sections. The dense parenchyma and fat tissue are well separated with this heavily T1-weighted acquisition. We used a

set of 67 patients to study the correlation between the 2-D projected percentage of dense area on a mammogram and the percentage of dense tissue volume estimated from the 3-D MR images.

The mammograms consisting of the craniocaudal (CC) view and the mediolateral oblique (MLO) view of both breasts of the patient were digitized with a LUMISYS 85 laser film scanner at a pixel size of 50 μm×50 μm. The digitizer has a gray level resolution of 12 bits and a nominal optical density (O.D.) range of 0 to 4. For density segmentation, it is not necessary to use very high-resolution images. To reduce processing time, the full resolution mammograms were first smoothed with a 16×16 box filter and subsampled by a factor of 16, resulting in 800 μm×800 μm images for this study.

B. Estimation of fibroglandular tissue volume on MR images

Since it is not our intention to routinely segment MR images for breast density estimation, we did not attempt to develop an automated method for this application. Our algorithm for segmentation of volumetric fibroglandular tissue on MR images used a semi-automatic method. The computer performed an initial segmentation. A graphical user interface (GUI) was developed to allow a user to review the segmentation of every slice and make modifications if necessary. The method consists of four steps. First, the breast boundary was detected automatically on each slice. A deformable model and manual modification were used to correct for incorrectly detected boundaries that usually occurred in slices near the chest wall where there were no well-defined breast boundaries. Because of inhomogeneity of the breast coil sensitivity, the signal intensity in the breast region was not uniform across the field of view. A background correction technique that estimated the low frequency background from the gray levels along the breast boundary was developed to reduce this systematic nonuniformity. Manual interactive thresholding of the gray level histogram in the breast region was then used to separate the fibroglandular from the fatty region. Morphological erosion was used to exclude the skin voxels along the breast boundary. Finally, the volume of fibroglandular tissue was calculated by integration over all slices containing the breast. A flow chart of our algorithm is shown in Fig. 1.

C. Breast boundary detection

A two-step algorithm was developed for the detection of breast boundary on each slice. First, we used a seeded pixel thresholding algorithm (SPTA) for the initial assessment of a breast boundary. Second, a 2-D active contour algorithm further refined the boundary. For slices close to the chest wall where no clear boundary can be seen, manual modification was used to outline an estimated boundary.

The SPTA determined the optimal threshold by iteratively partitioning the MR image into two parts and using the gradient value along the boundary of the partition as a guide in optimizing the threshold. First, the center of gravity was se-
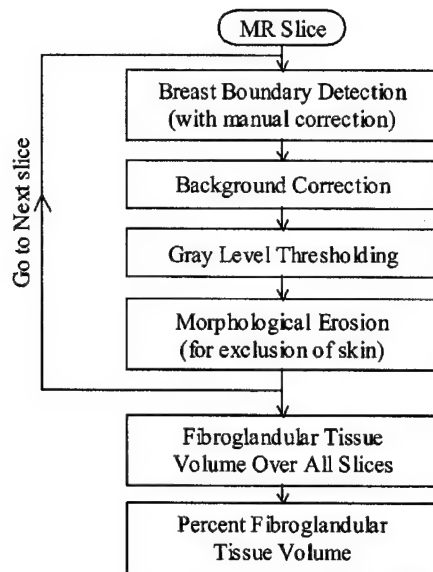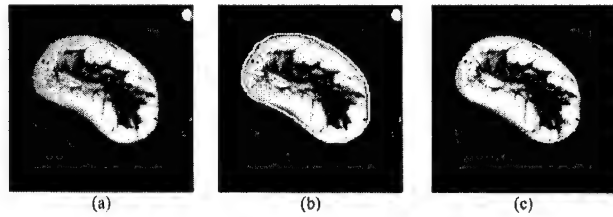
FIG. 2. An example of the first three processing blocks in Fig. 1. (a) Original MR slice; (b) automatically-detected breast boundary superimposed on the image; and (c) the background-corrected image.

FIG. 1. The flow-chart for the segmentation of the fibroglandular tissue on MR images.

$$E_{exert} = w_{grad}E_{grad}(c) + w_{bal}E_{bal}(c), \tag{3}$$

where curv, cont, grad, bal, hom denoted curvature, continuity, gradient, balloon force and homogeneity, respectively, and each energy term was associated with a weight, w. The detailed definition for each term can be found in the literature.[35] An example of a MR slice of a breast is shown in Fig. 2(a), and the segmented boundary is shown in Fig. 2(b). Note that the two breasts of a patient were scanned together but each breast was analyzed separately.

D. Background correction

To reduce the nonuniformity of the MR signal intensity in the breast region, a background correction technique[36] using the pixel values around the segmented breast region was employed. For a given pixel (i,j) inside the breast region, the gray value of the background image was estimated as shown in Eq. (4):

$$B(i,j) = \left[\frac{L}{d_l} + \frac{R}{d_r} + \frac{U}{d_u} + \frac{D}{d_d} \right] \bigg/ \left[\frac{1}{d_l} + \frac{1}{d_r} + \frac{1}{d_u} + \frac{1}{d_d} \right], \tag{4}$$

where L, R, U and D are the average gray values inside a breast background estimation region (BBER) centered at the left, right, upper and lower pixels on the breast boundary, respectively. A BBER was defined as the intersection of a 21×21-pixel box and the breast region. The center pixels for the left and right boxes were the intersection points between the breast boundary and a horizontal line passing through the given pixel (i,j). Similarly, the upper and lower center pixels for the upper and lower boxes were the intersection points between the breast boundary and a vertical line passing through the given pixel (i,j). Only the pixels that were within the intersected area between the 21×21-pixel box and the breast region were included in the definition of the BBER and the calculation of the average gray value. The contributions of the average gray levels to the background pixel (i,j) were inversely weighted by their distances d_l, d_r, d_u, d_d from the given pixel (i,j). An example of the background corrected image is shown in Fig. 2(c).

E. Segmentation of fibroglandular tissue

We developed a GUI that allowed the user to perform a combination of manual and automatic operations to segment the breast boundary and the fibroglandular tissue on the MR

lected as the starting pixel on each slice. The gray level of the starting pixel was used as a threshold to create a binary partition of the image in which all pixels greater than the threshold were set to one and all other pixels were set to zero. Second, the gradient value of each pixel on the boundary of the binary partition was calculated by applying the Sobel filter to the original image. The gradient assessment for this particular binary partition was defined as the average gradient magnitude of these boundary pixels. The threshold value was reduced to zero in a stepwise manner. The partition for each threshold value was created and the gradient assessment for each partition was calculated as described above. The partition with the maximum gradient assessment was considered to be the initial segmentation result for the breast, and the boundary of this partition was considered to be the initial breast boundary.

After the initial segmentation, a deformable contour method was used to further refine the boundary. The movement of the boundary pixel was controlled by an energy function which consisted of internal energy and external energy. The internal energy components used in this study were the continuity and curvature of the contour, as well as the homogeneity of the segmented partition. The external energy components were the negative of the smoothed image gradient magnitude, and a balloon force that exerted pressure at a normal direction to the contour. The energy function was defined as the following:

$$E = \sum_{c=1}^{N} \left[E_{inter}(c) + E_{exert}(c) \right], \tag{1}$$

where E_{inter} and E_{exert} are the internal energy and the external energy, respectively, as defined in Eq. (2) and Eq. (3):

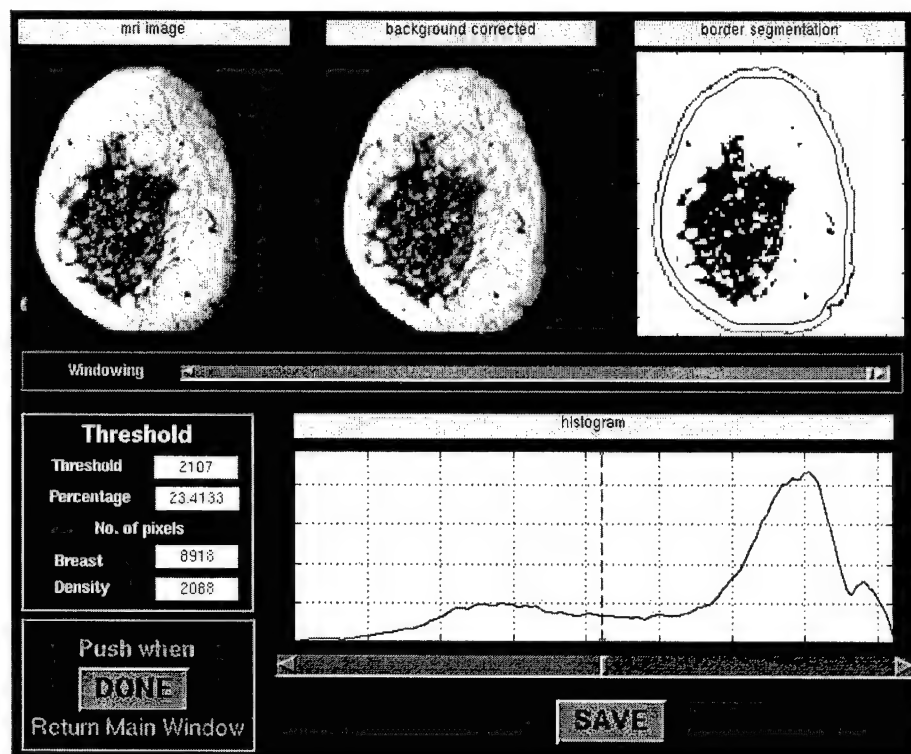$$E_{inter} = w_{curv}E_{curv}(c) + w_{cont}E_{cont}(c) + w_{hom}E_{hom}, \tag{2}$$

FIG. 3. The graphic user interface for the segmentation of the fibroglandular tissues on the MR slice. The upper row shows the original MR slice (left), the background-corrected image (middle) and the segmented binary image (right). The segmented image responds to the reader's adjustment of the gray level threshold (lower row) in real time so that the reader can choose the appropriate threshold by inspecting the segmented image visually. The dark area in the segmented image indicates the fibroglandular tissue and the white area indicates the adipose tissue. The inner line along the breast boundary is the boundary obtained by morphological erosion to exclude the skin voxels for calculating the fibroglandular tissue volume.

images. The first window (not shown) displayed the MR series and the corresponding mammogram of each breast to give the user an overview of the breast. The segmentation of the fibroglandular tissue on each MR slice was processed in the second window, shown in Fig. 3. The original MR slice, the corresponding background corrected image and the segmented binary image were shown in the upper part of the window. At the lower part of the window, the histogram of the voxel values in the breast region was shown. The user performed interactive thresholding on the histogram and the segmented binary image corresponding to the chosen threshold was displayed in real time in the upper part. If the breast boundary, which was automatically segmented by the computer initially, had to be corrected, the user could go to the third window and manually move the apices of the polygon outlining the boundary. The voxels contributed by the nipple were excluded. On the slices containing breast skin that had voxel values similar to those of fibroglandular tissue, a morphological erosion operation was applied to the breast boundary to exclude the skin voxels from the calculation of the fibroglandular tissue volume in the slice. The size of the structuring element could be selected interactively on the fourth window and the eroded boundary was displayed instantly for a chosen erosion operation. The user might again change the structuring element if the erosion result of the previous choice was deemed unsatisfactory. Since the eroded boundary only marked the region within which the fibroglandular voxels would be summed and would not be used for the calculation of the breast volume, as described below, it did not need to be precise as long as it excluded the skin voxels while not excluding the fibroglandular voxels.

F. MR fibroglandular tissue volume

After the fibroglandular tissue was segmented for each slice, the total number of voxels containing the fibroglandular tissue was obtained as a summation of these voxels over all slices of the breast. The total volume of the breast was obtained as the summation of the voxels enclosed by the breast boundary before morphological erosion. The ratio of these two volumes provided the percent volumetric fibroglandular tissue in the breast.

G. Mammographic density segmentation

We have previously developed an automated method for segmentation of the dense fibroglandular area on mammograms. The method, referred to as the Mammographic Density ESTimator (MDEST) was described in detail elsewhere.[32] In brief, the breast boundary on the digitized mammogram is tracked. A dynamic-range compression technique reduces the gray level range of the breast area. By analyzing the shape of the gray level histogram, a rule-based classifier classifies the breast density into one of four classes. Typically, a Class I breast is almost entirely fat; it has a single narrow peak on the histogram. A Class II breast contains scattered fibroglandular densities. Its histogram has two main peaks, with the smaller peak on the right of the bigger one. A Class III breast is heterogeneously dense. Its histogram also has two peaks, but the smaller peak is on the left of the bigger one. A Class IV breast is extremely dense. Its histogram has mainly a single dominant peak, but the peak is wider compared with the peak in the Class I histogram. A second smaller peak sometimes occurs on the left of the
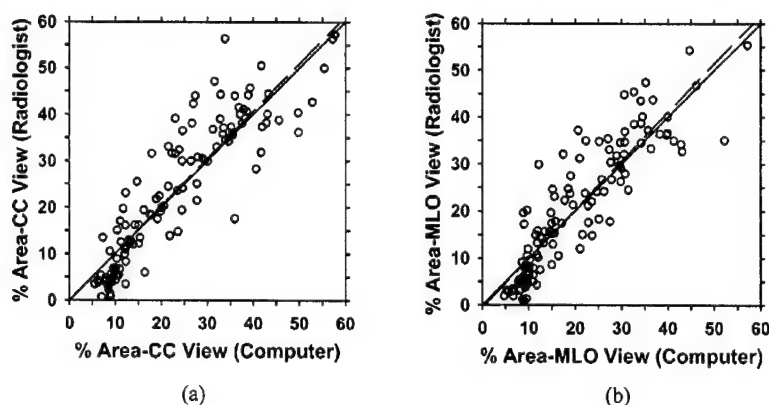
FIG. 4. A comparison of the percent mammographic density obtained from interactive thresholding by an MQSA-qualified radiologist and that estimated by our automated MDEST computer program. (a) CC view, correlation coefficient=0.90, rms residual=6.7, mean difference=0.3; (b) MLO view, correlation coefficient =0.89, rms residual=6.1, mean difference=0.4. Dashed line: linear regression of the data; solid line: diagonal.

main peak. Based on the histogram shape, a threshold is automatically calculated to separate the dense and fatty pixels. The mammographic density was estimated as the percentage of fibroglandular tissue area relative to the total breast area. For MLO view mammograms, the pectoral muscle is detected and excluded from the density area or breast area calculations. In our previous work, the performance of MDEST was verified by comparison with manual segmentation by 5 breast imaging radiologists using a dataset of 260 mammograms from 65 patients that were different from the cases used in the current study. We found that the correlation between the computer-estimated percent dense area and the average segmentation by the 5 radiologists was 0.94 and 0.91, respectively, for CC and MLO views, with a mean bias of less than 2%.

MDEST was applied to the mammograms of the 67 patients used in this study. The percent dense area on mammograms was estimated for the CC-view and the MLO-view mammogram of each breast separately. In addition, an MQSA-qualified radiologist also segmented the dense area by interactive thresholding for each mammogram. The correlation between the mammographic density obtained by manual and automatic segmentation is shown in Figs. 4(a) and 4(b) for the CC view and MLO view, respectively. The correlation coefficients for the CC view and MLO view were 0.90 and 0.89, respectively. The mammographic densities estimated by automatic and manual segmentation were compared with the percent volumetric fibroglandular tissue on MR images as described below.

H. Observer experiments

We performed an experiment to evaluate the variability of the estimated % volumetric fibroglandular tissue due to the uncertainty in the determination of the starting slice of the breast at the chest wall. The starting slice affected the estimation of the breast volume that was calculated by integrating from the starting slice to the anterior of the breast. Twenty-three MR cases from the dataset were randomly selected for this observer experiment. There were a total of 41 breasts because some cases had only one breast. For this subset of cases, each radiologist was asked to select the starting slice from the MR images for each breast. The estimated

% volumetric fibroglandular tissue calculated with all available slices was then compared to that calculated with the selected starting slice.

We also performed observer experiments to evaluate the inter-observer variations in the segmentation of fibroglandular tissue using the semi-automatic method. Two MQSA-qualified radiologists performed the segmentation of the fibroglandular tissue on the MR images of the 41 breasts using the semi-automatic method implemented with the GUI. A Ph.D. researcher who was trained by these radiologists also performed the segmentation independently with the GUI.

After verifying the consistency of segmentation by these observers, the trained Ph.D. completed the segmentation of all MR cases. The correlation between percent volumetric fibroglandular tissue on MR images and percent dense area on mammograms was then examined for the entire dataset.

III. RESULTS

A. Effect of selection of the starting slice

Figure 5(a) shows the correlation of the % volumetric fibroglandular tissue calculated using all available slices for the breast with that calculated using the selected starting slice by radiologist A for the 41 breasts. The correlation coefficient was 0.999. To compare the difference between their results, the mean difference and the root-mean-square (rms) residual, which is the residual from the linear least-squares-fitted line, were also calculated. The mean difference was 0.7 and the rms residual was 0.6. The result is similar for radiologist B (not shown), with a correlation coefficient of 0.999, a mean difference of 0.4 and a rms residual of 0.4. The correlation between the % volumetric fibroglandular tissue calculated using the selected starting slice by radiologist A with that calculated using the selected starting slice by radiologist B was also very high with a correlation coefficient of 0.988, a mean difference of 0.7 and a rms residual of 1.8, as shown in Fig. 5(b). These comparisons indicated that the variability in the selection of the starting slice of the breasts did not have a strong influence on the % volumetric fibroglandular tissue. We therefore used all available slices in the MR dataset for each breast in the following analyses.
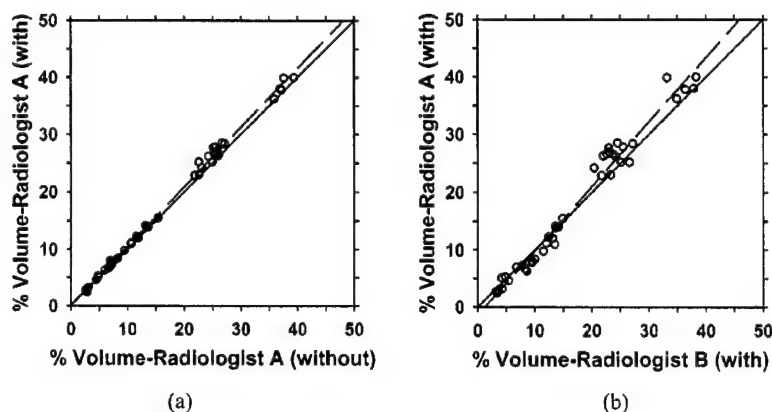
FIG. 5. (a) A comparison of the percent fibroglandular tissue volume calculated using the selected starting slice with that calculated using all available slices for radiologist A, correlation coefficient = 0.999. (b) A comparison of the percent fibroglandular tissue volume calculated using the selected starting slice by radiologist B with that by radiologist A, correlation coefficient = 0.988, Dashed line: linear regression of the data; solid line: diagonal.

B. Inter-observer variation between radiologists

Figure 6(a) shows the comparison of the percent volumetric fibroglandular tissues on MR images segmented by two radiologists for the 41 breasts. The correlation between the segmentation results of the two radiologists is 0.99. The mean difference was found to be 0.3 and the rms residual was 1.6.

C. Inter-observer variation between radiologists and trained Ph.D.

Figure 6(b) shows the comparison of the percent volumetric fibroglandular tissues segmented by the trained Ph.D. against that segmented by radiologist A. A similar result was obtained by comparing the percent volumetric tissue segmented by the trained Ph.D. and that segmented by radiologist A except that the data points were even closer to the diagonal (not shown). The correlation between the result of the trained Ph.D. and the results of both radiologists was 0.99. The corresponding mean differences were −0.8 and −0.4, respectively, and the rms residuals were 1.4 and 1.5, respectively.

D. Correlation between percent volumetric fibroglandular tissue on MR images and percent mammographic density

The percent volumetric fibroglandular tissue on MR images was compared with the percent dense area on CC- and

MLO-view mammograms. After verifying that the difference in segmentation between the trained Ph.D. and the radiologists was similar to the interobserver variations between the two experienced radiologists, the trained Ph.D. completed the segmentation of the entire dataset.

Figure 7 shows the comparison of the percent volumetric fibroglandular tissue on MRI and the percent mammographic density segmented by a radiologist. The percent areas on CC- and MLO-view mammograms are higher than the percent volume on MR images with a mean difference of 5.7% and 3.0%, respectively.

Figure 8 shows the comparison of the percent volumetric fibroglandular tissue on MRI and the percent mammographic density segmented by MDEST. The percent areas on CC- and MLO-view mammograms segmented by the computer are higher than the percent volume on MR images with a mean difference of 5.3% and 2.6%, respectively.

The correlation coefficients, the mean differences and the rms residuals between the percent volumetric fibroglandular tissue on MR images and percent dense area on mammograms are compared in Table. I. The correlation between the percent volume on MR images and percent area on mammograms of the fibroglandular breast tissue is high, ranging from 0.89 to 0.91. Although it is not expected that the values of percent volume agree with the values of percent area, their mean differences range only from 3% to 6% and the rms residual range from 5.4 to 6.3.
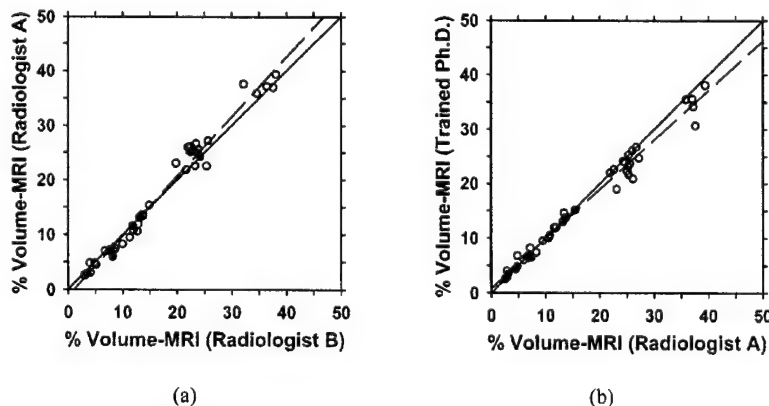

FIG. 6. A comparison of the segmentation of fibroglandular tissue from MR images between two observers: (a) two experienced MQSA-qualified radiologists, correlation coefficient = 0.99. (b) The trained Ph.D. and Radiologist A, correlation coefficient = 0.99. The correlation between the trained Ph.D. and Radiologist B is also 0.99 but the data points were very close to the diagonal and is not shown. The % volumetric fibroglandular tissue was calculated using all available slices. Dashed line: linear regression of the data; solid line: diagonal.
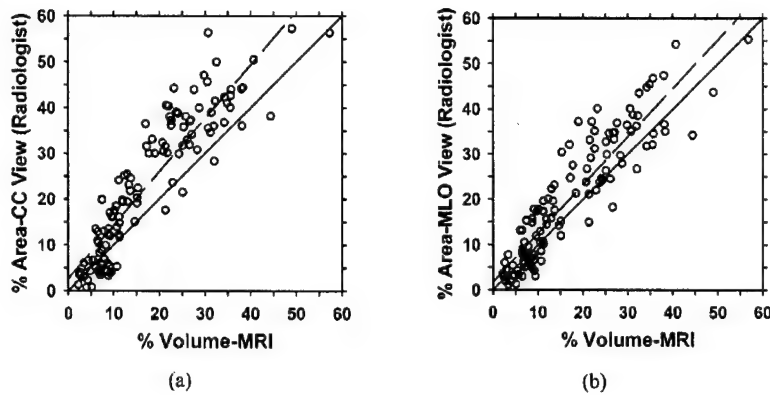
FIG. 7. A comparison of the percent fibroglandular tissue volume on MR images and the percent dense area on mammograms segmented by an experienced radiologist. (a) CC view, correlation coefficient=0.91; (b) MLO view, correlation coefficient=0.91. Dashed line: linear regression of the data; solid line: diagonal.

IV. DISCUSSION

Our purpose in this paper was to investigate the relationship between the percent dense area on mammogram and the percent fibroglandular tissue volume on MR image. We found a direct correlation between mammographic density and MR volumetric density (Fig. 7 and Fig. 8). The correlation coefficients between the percent area on a mammogram and the percent volume on MR images are high at 0.89 and 0.91. These results are more promising than those found in previous studies that attempted to correlate percent dense area on mammograms with MR information. Graham *et al.*[33] investigated the relationship between percent density (projected dense area) on mammogram and two objective MR parameters of breast tissue, relative water content and mean T2 relaxation. Their results with 45 cases showed a positive correlation between percent density and relative water content (Pearson correlation coefficient=0.79) and a negative correlation between percent density and mean T2 value (Pearson correlation coefficient= −0.61). Another study by Lee *et al.*[34] analyzed fatty and fibroglandular tissue in different age groups to compare x-ray mammography with T1-weighted MR images. Their study with 40 cases indicated that the correlation between the two techniques is 0.63 when the fat content was more than 45%. However, the correlation coefficient decreased to 0.34 when their analysis included only dense breasts.

It may be noted that although MR imaging is currently the most accurate method for estimating the volumetric fibro-

glandular tissue in the breast, it is still not the ideal tool. Fibrous tissue and glandular tissue are not well separated with current MR imaging techniques. Since the amount of glandular tissue in the breast is the important factor relating to breast cancer risk, further studies are warranted for differentiating the glandular and the fibrous components of the imaged volume. The correlation between the percent glandular tissue volume and percent projected dense area on a mammogram will be a more reliable indicator of the usefulness of mammographic density analysis.

The density on mammograms is a 2-D projected area of the fibroglandular tissues. The percent dense area is not expected to be equal in value to the percent volume. The mean differences between the percent volume and the percent area on CC- and MLO-views, as determined by the radiologist's interactive segmentation, are 5.7 and 3.0, respectively (Table I), with the percent dense area values being higher. We also investigated the rms residual between the percent volume and the percent area when the relationship between them was assumed to be linear. The rms residual between the percent volume and the percent area on CC- and MLO-views are 6.3 and 5.6, respectively (Table I), relative to the straight line obtained from linear least squares fits to the data. One possible factor that may contribute to a higher value of percent dense area on mammograms than the percent volume value on MR images is that the tissue volume imaged by the two modalities is somewhat different. The MR images include more tissue near the chest wall, which is mainly retroglan-
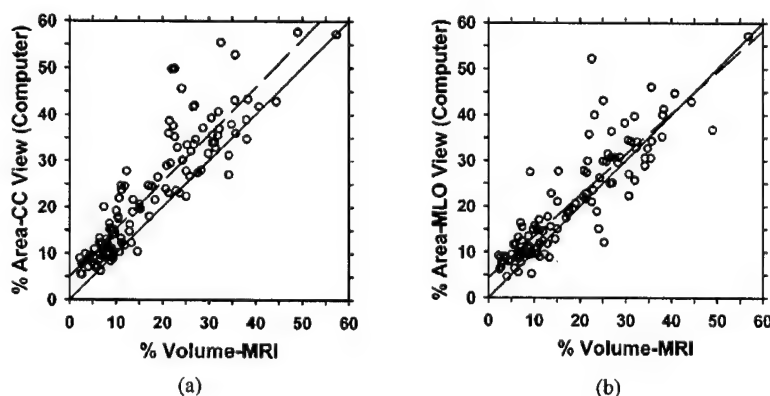

FIG. 8. A comparison of the percent volume on MR images and the percent area on mammogram segmented by our automated MDEST computer program. (a) CC view, correlation coefficient=0.91; (b) MLO view, correlation coefficient=0.89. Dashed line: linear regression of the data; solid line: diagonal.

TABLE I. Statistic analysis of the relationship between percent fibroglandular tissue volume on breast MR images and percent dense area on mammograms segmented by radiologist and MDEST.

	Radiologist		Computer (MDEST)	
	CC vs MRI	MLO vs MRI	CC vs MRI	MLO vs MRI
Correl. coeff.	0.91	0.91	0.91	0.89
rms residual	6.3	5.6	5.8	5.4
Mean diff.	5.7	3.0	5.3	2.6

TABLE II. An analysis of the relationship between percent fibroglandular tissue volume (x) on breast MR images and percent dense area (Y) on mammograms segmented by radiologist using three mathematical models. m, k, k_1 and k_2 are constants determined by least squares curve fitting.

Mathematical model		$Y = kx^{2/3}$	$Y = kx^m$	$Y = k_1 x^m + k_2$
CC vs MRI	Least squares Fit	$Y = 0.82x^{2/3}$	$Y = 1.03x^{0.83}$	$Y = 1.02x^{0.48} - 0.19$
	rms residual	6.5	6.0	5.6
	Coefficient of determination	0.82	0.85	0.87
MLO vs MRI	Least squares Fit	$Y = 0.73x^{2/3}$	$Y = 0.96x^{0.86}$	$Y = 0.90x^{0.60} - 0.09$
	rms residual	6.0	5.5	5.3
	Coefficient of determination	0.80	0.84	0.85

dular adipose tissue, than a mammogram does, thus reducing the percentage of fibroglandular tissue volume. The reduction in the percent volume values, however, is relatively small, as found in our study evaluating the effects of selecting starting slices for volume calculation (Fig. 5). The main difference may therefore be attributed to the geometric relationship between the volume and the projected 2-D area, explained later.

Geometrically, we do not expect the relationship between volume and its projected 2-D area to be linear. In a hypothetical situation such that the dense tissue volume is a sphere (volume=4/3 πr^3) enclosed inside a concentric spherical shell of fatty tissue volume, the percent projected 2-D area (area= πr^2) of the inner sphere relative to the outer sphere is equal to the percent volume to the power of 2/3. The relationship between the percent area and the percent volume is therefore not linear, and the percent area is larger in value than the percent volume for any ratio of radii between the two spheres. In general, the compressed breast and the dense tissue are not spherical. To investigate the empirical relationship between the percent area and the percent volume in the nonlinear situation, we applied least squares fits in several polynomial models to the data points in Fig. 7. The results are shown in Table II and Fig. 9. A comparison of Table I and Table II indicates that the $Y = kx^{2/3}$ model (x=percent fibroglandular tissue volume, Y =percent mammographic dense area) resulted in slightly larger rms residuals than the linear model. The model $Y = kx^m$ with m equal to 0.83 and 0.86, respectively, for CC- and MLO-views slightly reduced the rms residuals. The best fit was obtained from the model $Y = k_1 x^m + k_2$. However, the

situation that the percent projected area was negative when the percent volume was zero would not occur physically. Note that if the model was fitted to the percent area data segmented by MDEST (Fig. 8), the k_2 values would become positive, indicating that the nonzero k_2 values are likely caused by segmentation biases.

Overall, these models demonstrate that there is no simple mathematical relationship between the percent volume and the percent projected area but the values for the exponents appeared to be in a reasonable range. The relationship between the percent volumes of two 3-D objects, one within another, and their percent projected 2-D area depends on their shapes. For example, the closer the two volumes are to concentric cylinders of the same height, the closer the exponent is to unity. The spread of the data points can therefore be attributed to the various irregular shapes of the fibroglandular tissue in the breasts, the changes in the shapes of the fatty and fibroglandular tissue due to compression, as well as the uncertainties in the segmentation of both the mammograms and the MR images. Although the spread of the data points in the correlation plots is large, one can expect that when the mammographic density of a given patient is monitored over time, the variations in the projected dense area due to the geometric factors, described above, will actually be much less than that observed from the scatter plots among a large number of patients. In other words, the uncertainty in the estimated percent density from the serial mammograms of a given patient should be much less than those shown in
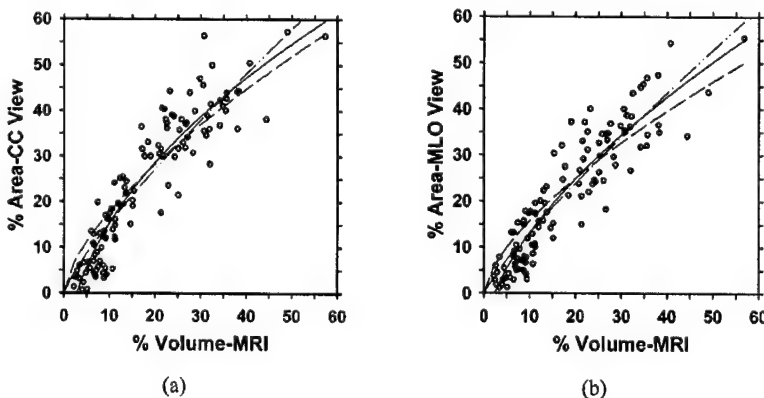

FIG. 9. Nonlinear fitting of the relationship between the percent volume and the percent area segmented by a radiologist with the least squares method. (a) CC view, (b) MLO view. Dashed line: $y = kx^{2/3}$; dashed–dotted–dotted line: $y = kx^m$; solid line: $y = k_1 x^m + k_2$. The fitted parameters of the models, m, k, k_1 and k_2, are shown in Table II.

(a)   (b)

Fig. 7. The strong correlation observed between the percent dense area on mammograms and the percent volumetric fibroglandular tissue on MR images therefore indicates that a change in mammographic density can be a useful indicator of a change in percent fibroglandular tissue volume in the breast.

Recently, some researchers attempted to estimate the thickness of the fibroglandular tissue in local regions of the mammograms from the projected density.[37] This approach is expected to provide a more accurate estimation of the fibroglandular tissue volume if the true thicknesses of the fibroglandular tissue and fatty tissue can be determined at various locations of the projected breast region. The volume of the fibroglandular tissue can then be summed over the pixels in the breast region and the percent volume calculated. However, to obtain accurate measurements, this approach requires the knowledge of the sensitometric curve for the screen-film mammogram at the imaging facility (or use of a digital detector with linear response) and other physical parameters such as the scatter fraction, the beam quality and beam hardening, in addition to the compressed breast thickness and the breast shape profile at the periphery. Some of the requirements may be circumvented by using a look-up table predetermined with a phantom calibration. Other factors may have to be approximated or ignored, or require further corrections by imaging each mammogram with a calibration phantom placed adjacent to the breast. This method is still being developed and the accuracy of estimating the thickness of the local fibroglandular tissue from a mammogram is yet to be determined. To our knowledge, no study to date has demonstrated that fibroglandular tissue volume estimated from mammograms has a higher correlation with the percent volumetric fibroglandular tissue volume estimated from MR images or other volumetric methods than we found in our current study. Furthermore, even if the local fibroglandular tissue thickness on mammograms can be measured in a laboratory or in an academic center using elaborate calibration schemes, it is doubtful that these methods can be translated into routine clinical measurement in mammography clinics. Its use may then be limited to controlled clinical trials. An estimation of the percent dense area projected on mammograms is likely a more practical approach for breast density assessment. The high correlation between the percent dense area and the percent fibroglandular tissue volume on MR images as demonstrated in the current study further supports the validity of this approach.

V. CONCLUSION

In this study, we investigated the correlation between the percent mammographic dense area and the percent volumetric fibroglandular tissue as measured on MR images. A semi-automatic method was developed for segmentation of the MR images and a fully automated computerized method, MDEST, was used to segment the mammograms. The performance of MDEST on the set of mammograms used in this study was verified with an experienced radiologist's manual segmentation. The inter-observer variability in segmentation

of MR images was found to be small with correlation coefficients of 0.99. The correlation between the percent volume on MR images and percent area segmented by a radiologist for either CC- view or MLO-view is 0.91. The correlation between percent volume and percent area estimated by MDEST is 0.91 and 0.89, respectively, for CC and MLO views. Mammographic density is thus highly correlated with the percent volumetric fibroglandular tissue in the breast. The high correlation indicates that changes in mammographic density may be a useful indicator of changes in fibroglandular tissue volume in the breast. Our computerized image analysis tool, MDEST, can provide a consistent and reproducible estimation of percent dense area on routine clinical mammograms. The automated image analysis tool may improve the sensitivity of quantifying mammographic density changes, thereby contributing to the understanding of the relationship of mammographic density to breast cancer risk, detection, and prognosis, and the prevention and treatment of breast cancer.

ACKNOWLEDGMENTS

[a] Author to whom correspondence should be addressed. Jun Wei, Ph.D., Department of Radiology, University of Michigan, CGC B2103, 1500 E. Medical Center Drive, Ann Arbor, Michigan 48109. Phone: 734-647-8553; fax: 734-615-5513; electronic mail: jvwei@umich.edu

[1] A. F. Saftlas, R. N. Hoover, L. A. Brinton, M. Szklo, D. R. Olson, M. Salane, and J. N. Wolfe, "Mammographic densities and risk of breast cancer," Cancer (N.Y.) **67**, 2833–2838 (1991).

[2] N. F. Boyd, G. A. Lockwood, J. W. Byng, D. L. Tritchler, and M. J. Yaffe, "Mammographic densities and breast cancer risk," Cancer Epidemiology Biomarkers & Prevention **7**, 1133–1144 (1998).

[3] C. M. Vachon, C. C. Kuni, K. Anderson, V. E. Anderson, and T. A. Sellers, "Association of mammographically defined percent breast density with epidemiologic risk factors for breast cancer (United States)," Cancer Causes & Control **11**, 653–662 (2000).

[4] P. M. Krook, "Mammographic parenchymal patterns as risk indicators for incident cancer in a screening program: an extended analysis," Am. J. Roentgenolo. **131**, 1031–1035 (1978).

[5] R. L. Egan and R. C. Mosteller, "Breast cancer mammography patterns," Cancer (N.Y.) **40**, 2087–2090 (1977).

[6] B. Threatt, J. M. Norbeck, N. S. Ullman, R. Kummer, and P. Roselle, "Association between mammographic parenchymal pattern classification and incidence of breast cancer," Cancer (N.Y.) **45**, 2550–2556 (1980).

[7] M. Moskowitz, P. Gartside, and C. Mclaughlin, "Mammographic patterns as markers for high-risk benign breast disease and incident cancers," Radiology **134**, 293–295 (1980).

[8] I. Witt, H. S. Hansen, and S. Brunner, "The risk of developing breast cancer in relation to mammography findings," Eur. Radiol. **4**, 65–67 (1984).

[9] S. Ciatto and M. Zappa, "A prospective study of the value of mammographic pattern as indicators of breast cancer risk in a screening experience," Eur. Radiol. **17**, 122–125 (1993).

[10] E. Thurfjell, C. C. Hsieh, L. Lipworth, A. Ekbom, H. O. Adami, and D. Trichopoulos, "Breast size and mammographic pattern in relation to breast cancer risk," Eur. J. Cancer Prevention **5**, 37–41 (1996).

[11] I. Kato, C. Beinart, A. Bleich, S. Su, M. Kim, and P. G. Toniolo, "A nested case-control study of mammographic patterns, breast volume and

breast cancer (New York City, NY, United States)," Cancer Causes & Control **6**, 431–438 (1995).

[12] E. Sala, R. Warren, J. McCann, S. Duffy, N. Day, and R. Luben, "Mammographic parenchymal patterns and mode of detection: implications for the breast screening programme," J. Medical Screening **5**, 207–212 (1998).

[13] T. M. Salminen, I. E. Saarenmaa, M. M. Heikkila, and M. Hakama, "Is a dense mammographic parenchymal pattern a contraindication to hormonal replacement therapy?," Acta Oncol. **39**, 969–972 (2000).

[14] C. Byrne, C. Schairer, J. N. Wolfe, N. Parekh, M. Salane, L. A. Brinton, R. Hoover, and R. Haile, "Mammographic features and breast cancer risk: Effects with time, age, and menopause status," J. Natl. Cancer Inst. **87**, 1622–1629 (1995).

[15] N. F. Boyd, C. Greenberg, G. Lockwood, L. Little, L. Martin, J. Byng, Y. Martin, and D. Tritchler, "Effects at two years of a low-fat, high-carbohydrate diet on radiologic features of the breast: Results from a randomized trial," J. Natl. Cancer Inst. **89**, 466–467 (1997).

[16] D. V. Spicer, G. Ursin, Y. R. Parisky, J. G. Pearce, D. Shoupe, A. Pike, and M. C. Pike, "Changes in mammographic densities induced by a hormonal contraceptive designed to reduce breast cancer risk," J. Natl. Cancer Inst. **86**, 431–436 (1994).

[17] J. Brisson, R. Verreault, A. S. Morrison, D. Tennina, and F. Meyer, "Diet, mammographic features of breast tissue, and breast cancer risk," Am. J. Epidemiol. **130**, 14–24 (1989).

[18] J. N. Wolfe, "Mammography: Ducts as a sole indicator of breast carcinoma," Radiology **89**, 206–210 (1967).

[19] J. N. Wolfe, "The prominent duct pattern as an indicator of cancer risk," Oncology **23**, 149–158 (1969).

[20] J. N. Wolfe, "Breast patterns as an index of risk for developing breast cancer," Am. J. Roentgenol. **126**, 1130–1139 (1976).

[21] J. N. Wolfe, "Risk for breast cancer development determined by mammographic parenchymal pattern," Cancer (N.Y.) **37**, 2486–2492 (1976).

[22] I. E. Magnin, F. Cluzeau, C. L. Odet, and A. Bremond, "Mammographic texture analysis: An evaluation of risk for developing breast cancer," Opt. Eng. **25**, 780–784 (1986).

[23] J. W. Byng, N. F. Boyd, E. Fishell, R. A. Jong, and M. J. Yaffe, "Automated analysis of mammographic densities," Phys. Med. Biol. **41**, 909–923 (1996).

[24] J. W. Byng, N. F. Boyd, E. Fishell, R. A. Jong, and M. J. Yaffe, "The quantitative-analysis of mammographic densities," Phys. Med. Biol. **39**, 1629–1638 (1994).

[25] M. J. Yaffe, N. F. Boyd, J. W. Byng, R. A. Jong, R. Fishell, G. A. Lockwood, L. E. Little, and D. L. Tritchler, "Breast cancer risk and measured mammographic density," Eur. J. Cancer Prevention **7**, S47–S55 (1998).

[26] Z. Huo, M. L. Giger, D. E. Wolverton, and W. Zhong, "Computerized analysis of mammographic parenchymal patterns for breast cancer risk assessment: Feature selection," Med. Phys. **27**, 4–12 (2000).

[27] J. J. Heine and R. P. Velthuizen, "A statistical methodology for mammographic density detection," Med. Phys. **27**, 2644–2651 (2000).

[28] J. M. Boone, K. K. Lindfors, C. S. Veatty, and J. A. Seibert, "A breast density index for digital mammograms based on radiologists' ranking," J. Digit Imaging **11**, 101–115 (1998).

[29] J. N. Wolfe, A. F. Saftlas, and M. Salene, "Evaluation of mammographic densities: A case-control study," Am. J. Roentgenol., Radium Ther. Nucl. Med. **148**, 1087–1092 (1987).

[30] *American College of Radiology. Breast Imaging—Reporting and Data System (BI-RADS)*, 3rd ed. (American College of Radiology, Reston, VA, 1998).

[31] E. White, P. Velentgas, M. T. Mandelson, C. D. Lehman, J. G. Elmore, P. Porter, Y. Yasui, and S. H. Taplin, "Variation in mammographic breast density by time in menstrual cycle among women aged 40–49 years," J. Natl. Cancer Inst. **90**, 906–910 (1998).

[32] C. Zhou, H. P. Chan, N. Petrick, M. A. Helvie, M. M. Goodsitt, B. Sahiner, and L. M. Hadjiiski, "Computerized image analysis: Estimation of breast density on mammograms," Med. Phys. **28**, 1056–1069 (2001).

[33] S. J. Graham, M. J. Bronskill, J. W. Byng, M. J. Yaffe, and N. F. Boyd, "Quantitative correlation of breast tissue parameters using magnetic resonance and x-ray mammography," Br. J. Cancer **73**, 162–168 (1996).

[34] N. A. Lee, H. Rusinek, J. Weinreb, R. Chandra, H. Toth, C. Singer, and G. Newstead, "Fatty and fibroglandular tissue volumes in the breasts of women 20–83 years old: comparison of x-ray mammography and computer-assisted MR imaging," Am. J. Roentgenol. **168**, 501–506 (1997).

[35] B. Sahiner, N. Petrick, H. P. Chan, L. M. Hadjiiski, C. Paramagul, M. A. Helvie, and M. N. Gurcan, "Computer-aided characterization of mammographic masses: Accuracy of mass segmentation and its effects on characterization," IEEE Trans. Med. Imaging **20**, 1275–1284 (2001).

[36] B. Sahiner, H. P. Chan, N. Petrick, D. Wei, M. A. Helvie, D. D. Adler, and M. M. Goodsitt, "Classification of mass and normal breast tissue: A convolution neural network classifier with spatial domain and texture images," IEEE Trans. Med. Imaging **15**, 598–610 (1996).

[37] O. Pawluczyk, B. J. Augustine, M. J. Yaffe, D. Rico, J. Yang, G. E. Mawdsley, and N. F. Boyd, "A volumetric method for estimation of breast density on digitized screen-film mammograms," Med. Phys. **30**, 352–364 (2003).

Performance evaluation of an automated breast density estimation system for digital mammograms and digitized film mammograms

Chuan Zhou, Heang-Ping Chan, Jun Wei, Mark A. Helvie, Marilyn A. Roubidoux, Chintana Paramagul, Alexis V. Nees, Lubomir M. Hadjiiski, Berkman Sahiner

Department of Radiology, University of Michigan, Ann Arbor, MI 48109
chuan@umich.edu

Abstract. Studies have demonstrated a strong correlation between mammographic breast density and breast cancer risk. We have previously developed a computerized system, mammographic density estimator (MDEST), to estimate breast density automatically on digitized film mammograms (DFM). In this study, we evaluated the performance of the MDEST system on full field digital mammograms (FFDM) and DFMs. The input to the system is a preprocessed dynamic range compressed image. The breast region is first segmented by breast boundary detection. The pectoral muscle is trimmed if it is an MLO view. A rule-based classifier is then used to classify the breast image into one of four classes according to the characteristics of its gray level histogram. The dense area from the breast region is subsequently segmented by automatic gray level thresholding. The breast density is estimated as the percentage of the segmented dense area relative to the breast area. In this study, two-view FFDM and the corresponding DFM from 99 patients with 202 images in each set were used. The dense area on each mammogram was segmented by 4 radiologists using interactive thresholding and their average was used as the "gold standard". The MDEST system was directly applied to the FFDM and DFM data without any re-training except that the preprocessing filter was modified for FFDMs. We found that the correlation between the estimated percent dense area and the gold standard was 0.850 and 0.873 on FFDM, and 0.885 and 0.824 on DFM, for CC and MLO views, respectively. The results demonstrated the feasibility of estimating breast density automatically on FFDM and DFM using the same MDEST system.

1. Introduction

Studies have demonstrated a strong correlation between breast density on mammograms and breast cancer risk (Saftlas and Szklo 1987; Brisson et al. 1989; Saftlas et al. 1991; Oza and Boyd 1993; Boyd et al. 1998; Yaffe et al. 1998). The relative risk is estimated to be about 4 to 6 times higher for women whose mammograms have parenchymal densities over 60% of the breast area, as compared to women with less than 5% of parenchymal densities. The strong correlation between breast density and breast cancer risk has prompted researchers to use mammographic density as an indicator for monitoring the effects of preventive or interventional treatment of breast cancer.

Because of the subjective nature of visual analysis, qualitative estimation may vary from radiologist to radiologist. A computerized method for measuring mammographic density would be useful as a supplement to the radiologist's assessment. We have previously developed a computerized system, mammographic density estimator (MDEST) (Zhou et al. 2001), to estimate breast density automatically on digitized film mammograms (DFM). The MDEST system performs dynamic range compression, breast boundary tracking, pectoral muscle trimming for MLO view, gray level thresholding based on histogram analysis, and calculation of the percent dense area on the mammogram. In the previous study, 260 digitized

4-view mammograms of 65 patients were used. The gold standard of percent dense area of the breast region for each mammogram was obtained by averaging five radiologists' manually segmented percent dense area. We found that the correlation between the computer-estimated percent dense area and radiologists' manual segmentation was 0.94 and 0.91, with RMS errors at 6.1% and 7.2%, respectively, for CC and MLO views.

In this study, we investigate the feasibility of computerized mammogramic density estimation on FFDMs and DFMs using the same image segmentation system. The MDEST system was directly applied to the FFDM and the corresponding DFM without any re-training except that the preprocessing filter was modified for FFDMs. The performance was evaluated by analyzing the correlation between the computer-estimated mammographic density and the gold standard obtained by radiologists' interactive thresholding.

2. Materials and Methods

The data sets consisting of FFDM and the corresponding DFM of 99 patients with 202 images in each set were used. Each case contains the craniocaudal (CC) view and the mediolateral oblique (MLO) view. The FFDM was acquired with a GE Senographe 2000D system and the raw GE FFDM was processed by a Laplacian pyramid multi-resolution preprocessing method (Wei et al. 2004). The preprocessed image was downsized to a pixel size of 800 μm x 800 μm image and 4096 gray levels. The DFM was acquired with mammography systems approved by the Mammography Quality Standards Act (MQSA) and was digitized with a LUMISYS 85 laser film scanner with a pixel size of 50 μm x 50 μm and 4096 gray levels. The digitized mammogram was also downsized to a 800 μm x 800 μm image using a 16x16 box filter.

Our previously developed computerized system MDEST was applied to the FFDMs and DFMs to estimate the mammographic density without any re-training. The density estimation was performed in three stages: breast region segmentation, image enhancement, and gray level thresholding based on histogram analysis . First, the breast region was segmented from the surrounding background by an automated breast boundary tracking algorithm for DFM. For FFDM, thresholding was used to separate the breast region from the background. Since our current pectoral muscle trimming program is not 100% accurate, the pectoral muscle was manually trimmed on the MLO view images for both DFM and FFDM in this study in order to separate the errors due to breast density segmentation from those due to pectoral muscle trimming. Second, an adaptive dynamic range compression technique was applied to enhance the DFM image. For FFDM image, a Laplacian pyramid multi-resolution preprocessing method (Wei et al. 2004) was used for image enhancement. At the third stage, for both FFDM and DFM, rule-based classification was used to classify the breast image into one of four classes according to the characteristic features of its gray level histogram (Zhou et al. 2001). For each image in the classified classes, a gray level threshold was determined adaptively to segment the dense area from the breast region. The breast density was estimated as the percentage of the segmented dense area relative to the breast area. As an example, typical mammograms in the four classes with the corresponding enhanced images, histograms, selected thresholds and the segmented image are shown in Figure 1. To evaluate the performance of MDEST, the computer segmentation results were compared to those by manual segmentation with interactive thresholding by four MQSA radiologists. The "gold standard" of percent dense area for each mammogram was obtained by averaging the manually segmented percent dense areas of the four radiologists.
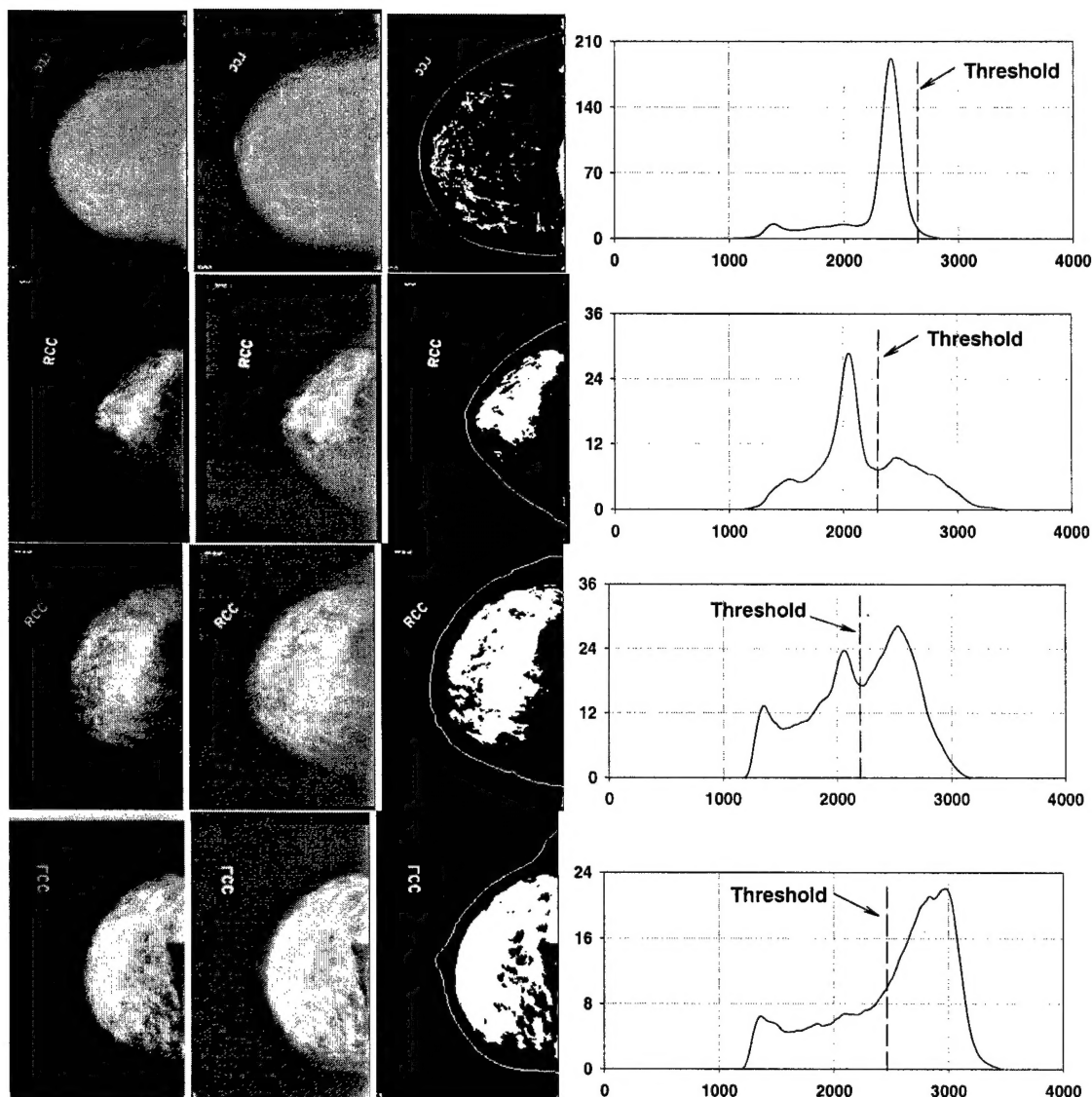
Figure 1. Typical mammograms in the four density classes and the corresponding enhanced and segmented images, histograms and thresholds. The columns from left to right correspond to the original image, enhanced image, segmented image and the histogram. Rows from top to bottom correspond to class one to four.

3. Results

Figures 2(a)-(d) show the comparison of the percent dense area between the estimation by the MDEST system and the gold standard on FFDM and DFM for CC- and MLO-view mammograms, respectively. Table 1 summarizes the comparison between the MDEST performance and the gold standard for FFDM and DFM, respectively. The correlation between the computer-estimated percent dense area and the gold standard is 0.850 and 0.873 on FFDM, and 0.885 and 0.824 on DFM, for CC and MLO views, respectively. For all of the images combining CC- and MLO-views, the correlation is 0.859 and 0.855 on FFDM and DFM, respectively. The RMS difference in the percent dense area between the MDEST estimation and the gold standard is 7.26%, 5.70% and 6.52% on FFDM, and 6.87%, 8.16%

and 7.54% on DFM for CC-view alone, MLO-view alone, and combined CC and MLO-views, respectively.

Table I. The correlation and RMS difference between the estimated percent dense area by the MDEST system and the gold standard (average of four MQSA radiologists).

Image subsets	FFDM		DFM	
	Correlation	RMS Error	Correlation	RMS Error
CC view	0.850	7.26%	0.885	6.87%
MLO view	0.873	5.70%	0.824	8.16%
All images	0.859	6.52%	0.855	7.54%

4. Conclusion

Our preliminary study demonstrated that the estimation of mammographic density could be performed efficiently by the automated image analysis tool. The computer-estimated percent dense area had a high correlation with the gold standard obtained from averaging four MQSA radiologists' manual segmentation. The results also demonstrated the feasibility of estimating breast density automatically on FFDM and DFM using the same MDEST system. Further study will be conducted to improve the breast density segmentation accuracy.
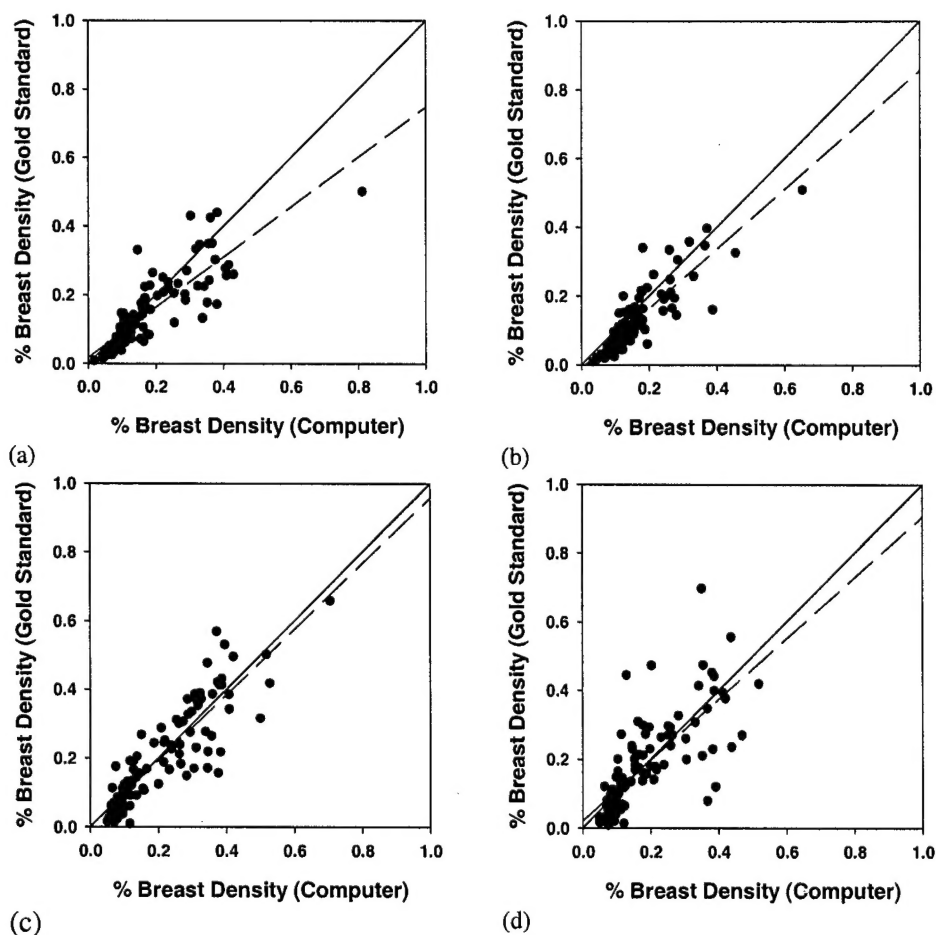
Figure 2. Comparison of the percent dense area between the estimation by the MDEST system and the gold standard. The dashed line represents the linear regression of the data on the plot. (a) FFDM CC view, (b) FFDM MLO view, (c) DFM CC view, (d) DFM MLO view.

References

Boyd, N. F., G. A. Lockwood, J. W. Byng, D. L. Tritchler and M. J. Yaffe. 1998. Mammographic densities and breast cancer risk. *Cancer Epidemiology Biomarkers & Prevention* 7:1133-1144.

Brisson, J., R. Verreault, A. S. Morrison, D. Tennina and F. Meyer. 1989. Diet, mammographic features of breast tissue, and breast cancer risk. *Am. J. Epidemiology* 130:14-24.

Oza, A. M. and N. F. Boyd. 1993. Mammographic parenchymal patterns: A marker of breast cancer risk. *Epidemiologic Reviews* 15:196-208.

Saftlas, A. F., R. N. Hoover, L. A. Brinton, M. Szklo, D. R. Olson, M. Salane and J. N. Wolfe. 1991. Mammographic densities and risk of breast cancer. *Cancer* 67:2833-2838.

Saftlas, A. F. and M. Szklo. 1987. Mammographic parenchymal patterns and breast cancer risk. *Epidemiologic Reviews* 9:146-174.

Wei, J., B. Sahiner, L. Hadjiiski, H. P. Chan, N. Petrick, M. A. Helvie, C. Zhou and Z. Ge. 2004. Computer aided detection of breast masses on full-field digital mammograms: false positive reduction using gradient field analysis. *Proc. SPIE Medical Imaging 2004: Image Processing* 5370:992-998.

Yaffe, M. J., N. F. Boyd, J. W. Byng, R. A. Jong, R. Fishell, G. A. Lockwood, L. E. Little and D. L. Tritchler. 1998. Breast cancer risk and measured mammographic density. *European J. of Cancer Prevention* 7, Suppl. 1:S47-S55.

Zhou, C., H. P. Chan, N. Petrick, M. A. Helvie, M. M. Goodsitt, B. Sahiner and L. M. Hadjiiski. 2001. Computerized image analysis: Estimation of breast density on mammograms. *Medical Physics* 28:1056-1069.